Feedback cooling of an insulating high-Q diamagnetically levitated plate

Feedback cooling of an insulating high-Q diamagnetically levitated plate

S. Tian ; K. Jadeja ; D. Kim ; A. Hodges ; G. C. Hermosa ; C. Cusicanqui ; R. Lecamwasam ;
J. E. Downes ; J. Twamley

Check for updates

View Online   Export Citation

Applied Physics Letters

AIP Publishing

Feedback cooling of an insulating high-Q diamagnetically levitated plate

View Online　　Export Citation　　CrossMark

S. Tian,[1] (iD) K. Jadeja,[1] (iD) D. Kim,[1] (iD) A. Hodges,[1] (iD) G. C. Hermosa,[2] (iD) C. Cusicanqui,[3] (iD) R. Lecamwasam,[1,4] (iD)
J. E. Downes,[5] (iD) and J. Twamley[1,a] (iD)

AFFILIATIONS

[1]Quantum Machines Unit, Okinawa Institute of Science and Technology Graduate University, Onna, Okinawa 904-0495, Japan
[2]Department of Chemical Engineering and Materials Science, Yuan Ze University, Chung-Li 32003, Taiwan
[3]Tecnologico de Monterrey, Escuela de Ingenieria y Ciencias, Monterrey 64849, Mexico
[4]A∗STAR Quantum Innovation Centre (Q.InC), Institute for Materials Research and Engineering (IMRE), Agency for Science,
 Technology and Research (A∗STAR), 2 Fusionopolis Way, 08-03 Innovis 138634, Republic of Singapore
[5]School of Mathematical and Physical Sciences, Macquarie University, Sydney, NSW 2109, Australia

[a]Author to whom correspondence should be addressed: jason.twamley@oist.jp

ABSTRACT

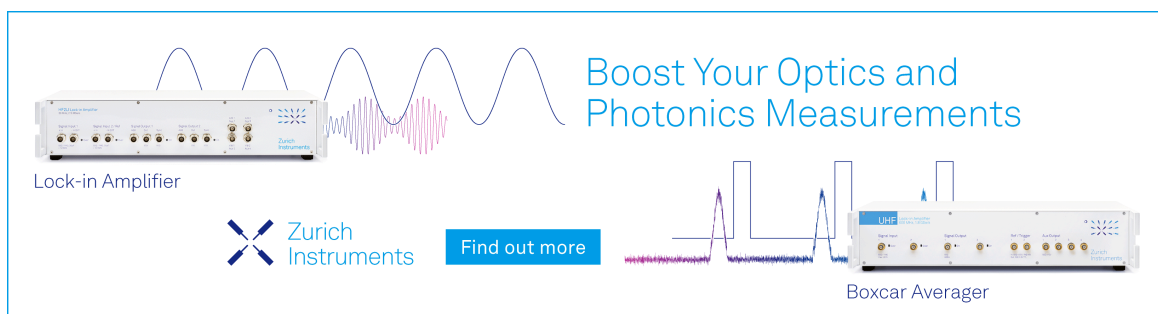Levitated systems in vacuum have many potential applications ranging from new types of inertial and magnetic sensors through to fundamental issues in quantum science, the generation of massive Schrödinger cats, and the connections between gravity and quantum physics. In this work, we demonstrate the passive, diamagnetic levitation of a centimeter-sized massive oscillator, which is fabricated using a method that ensures that the material, though highly diamagnetic, is an electrical insulator. Electrical conductors moving in a magnetic field experience eddy damping—which can severely reduce their motional quality factor. By chemically coating a powder of microscopic graphite beads with silica and embedding the coated powder in high-vacuum compatible wax, we form a centimeter-sized thin square plate which magnetically levitates over a checkerboard magnet array. The insulating coating reduces eddy damping by almost an order of magnitude compared to uncoated graphite with the same particle size. These plates exhibit a different equilibrium orientation from pyrolytic graphite due to their isotropic magnetic susceptibility. We measure the motional quality factor to be $Q \sim 1.58 \times 10^5$ for an approximately centimeter-sized composite resonator with a mean particle size of 12 μm. Furthermore, we apply delayed feedback to cool the vertical motion of frequency ∼19 Hz and achieve center-of-mass temperature decrease by three orders of magnitude.

Optomechanical systems are the most precise measuring devices in existence, most notably the LIGO gravitational wave observatory which can measure distortions in spacetime 10 000 smaller than a proton. Tabletop systems aim to exploit the versatile optomechanical interaction to design compact classical and quantum sensors. Optomechanical systems are fundamentally limited by thermal noise from the environment, which interferes with the measurement signal and causes decoherence of fragile quantum states. Levitated optomechanics suspends the system without any physical connection to the environment. The resulting exquisite isolation means that the quantum ground state of its harmonically confined motion can be attained at room temperature using feedback-cooling.[1] This is promising for both high-precision laboratory measurements and deployment in noisy real-world settings.[2,3] Levitation also leads to a natural coupling with gravity. Thus, levitated systems are natural testbeds for probing some of the deepest outstanding questions in physics, such as quantum gravity and gravity-induced wavefunction collapse mechanisms.[4]

Diamagnetic levitation of graphite slabs offers a unique platform for levitated optomechanics. Most levitated platforms use active methods, such as optical tweezers or Paul traps. These use time-varying optical or electromagnetic fields[2,3] and can trap particles of nano- and micro-meter sizes. In contrast diamagnetic levitation is passive, and centimeter-sized slabs of graphite can be easily levitated above an array of commercially available permanent magnets.[5–9] This removes the noise associated with an active power source.[10] Moreover, the lowered power and hardware requirements are promising for developing commercial sensors. Diamagnetic levitation can also support much larger masses than traditional levitated optomechanics. More massive

systems have greater sensitivity for accelerometry and gravimetry[11,12] and are crucial to explore the behavior of quantum physics at larger scales. The large mass, ease of use, and passive nature give graphite diamagnetic levitation a unique status in levitated optomechanics.

The greatest limiting factor for these systems is eddy damping. Most experiments use highly oriented pyrolytic graphite (HOPG), a synthetic material consisting of layered planes of graphite. This has a very strong diamagnetic susceptibility along the axis perpendicular to the graphite planes. However, HOPG is an electrical conductor. As it moves through the magnetic field generated by the magnets, currents are induced along the graphite planes, which cause strong damping. Consequently, the quality factor of levitated pyrolytic graphite in vacuum is only several hundred for millimeter-sized slabs and decreases as size increases.[9] Although a thin graphite film has demonstrated sufficient sensitivity to experimentally test theories of dark matter,[13] increasing the quality factor would substantially increase sensitivity and unlock powerful feedback-cooling methods.

It is, thus, necessary to find methods of suppressing eddy damping in levitated graphite systems. The currents can be disrupted by engineering narrow slits, allowing quality factors of several thousand in vacuum.[14,15] An alternative approach has been to use composite materials, consisting of micrometer-sized graphite particles dispersed in an insulating resin.[16] Eddy currents can only flow within the microparticles or between neighboring particles which happen to touch. In such systems, eddy damping depends only on the size of the particles and is independent of the overall size of the resonator. Millimeter-sized slabs of composite graphite attained quality factors of half a million at high vacuum at room temperature, the largest demonstrated for any system of that mass.[16]

Composite graphite is, thus, a highly promising system for levitated optomechanics. However, it also presents new challenges. Since the magnetic susceptibility of graphite is highly oriented, the random positioning of particles in the composite lowers the effective magnetic susceptibility. The susceptibility further decreases for particle sizes smaller than 30 μm,[17] though such sizes are necessary to significantly suppress eddy currents. Thus, the mass that can be supported is decreased, if, for example, we wished to place a mirror or other system on the levitated graphite. There is also a limit on the volume fraction of graphite in the material, which was about 40% in Chen *et al.*[16] for reasons of structural integrity. Moreover, the graphite particles must be kept separated by the insulating resin. At high volume fractions, it becomes increasingly likely that neighboring graphite particles will touch, allowing eddy currents to flow between them and, thus, decreasing the quality factor.

To enable large graphite volume fractions while maintaining suppression of eddy currents, we coat the graphite particles with an insulating shell. Our graphite particles are mesocarbon microbeads (MCMB), whose average diameter is 11 ± 2 μm. We chemically coat these with a thin insulating layer of silica in a "sol-gel process" using polyethylene glycol (PEG) and the silica precursor tetraethyl orthosilicate (TEOS)[18] (see the supplementary material for details on the fabrication process). First, PEG adsorbs onto the surface of the microcarbon microbeads. A solution of TEOS and ammonium hydroxide catalyst is then added and stirred for 17 h on a hot plate. During this time, silicon from TEOS attaches to the PEG, resulting in a silica coating on the graphite as shown in Fig. 1(a). The mixture is
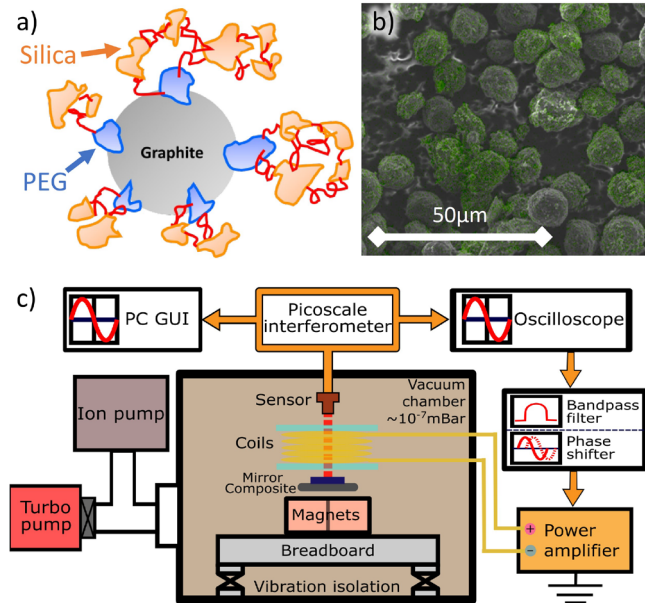

FIG. 1. Coated graphite and experimental setup. (a) We chemically coat each graphite particle with a layer of electrically insulating silica. Polyethylene glycol (PEG) works as a bridgemer, allowing silica to bind to the surface of the graphite. The coated graphite particles are mixed with vacuum-compatible wax and shaped into insulating diamagnetic slabs. (b) Scanning electron microscope image of the coated graphite microbeads, overlaid with energy-dispersive x-ray (EDX) elemental mapping. Green regions indicate silicon, confirming the presence of the insulating coating. (c) The insulating diamagnetic slab levitates above a checkerboard of four NdFeB magnets with orientation alternating between the north and south poles. The system is placed on a vibration–isolation platform and then kept in high vacuum ($10^{-6} - 10^{-7}$ mbar) (see Ref. 14 for more details of this setup). A mirror is fixed onto the slab for interferometric real-time measurement of the position and velocity. The delayed velocity signal is fed back after filtering and time delay through a coil of wire, which applies magnetic actuation to cool the vertical motion of the slab.

then washed, filtered, and dried. Analysis using scanning electron microscopy with elemental mapping shown in Fig. 1(b) confirms the near-uniform coverage of the graphite beads with silica. The powder is then mixed in vacuum-compatible wax at a temperature of approximately 150 °C, then cooled, and shaped into small square slabs of approximate width 8 mm and thickness 0.5 mm. We obtained a graphite mass fraction of 57% $\pm$ 2%, with the volume fraction estimated as 41% $\pm$ 2%. At larger volume fractions, mixing the graphite powder into the wax requires significant stirring force, which causes cracking of the silica shell.

The graphite slabs are levitated above a checkerboard-array of four permanent magnets, whose upper faces alternate between north and south poles. In Figs. 2(a) and 2(b), we show photographs of both pyrolytic and composite graphite, taken from above once their positions had reached equilibrium. We can see that the pyrolytic and composite graphite exhibit different orientations. This arises from the difference in their magnetic susceptibilities. The potential energy of a diamagnet in a magnetic field is given by

$$U_B(z, \phi) = -\frac{1}{2\mu_0} \int_{\mathcal{V}(z,\phi)} \left[\chi_x B_x^2 + \chi_y B_y^2 + \chi_z B_z^2 \right] dx \, dy \, dz. \quad (1)$$

HOPG

Composite

Equilibrium orientation of plate above magnets

Magnetic potential energy density
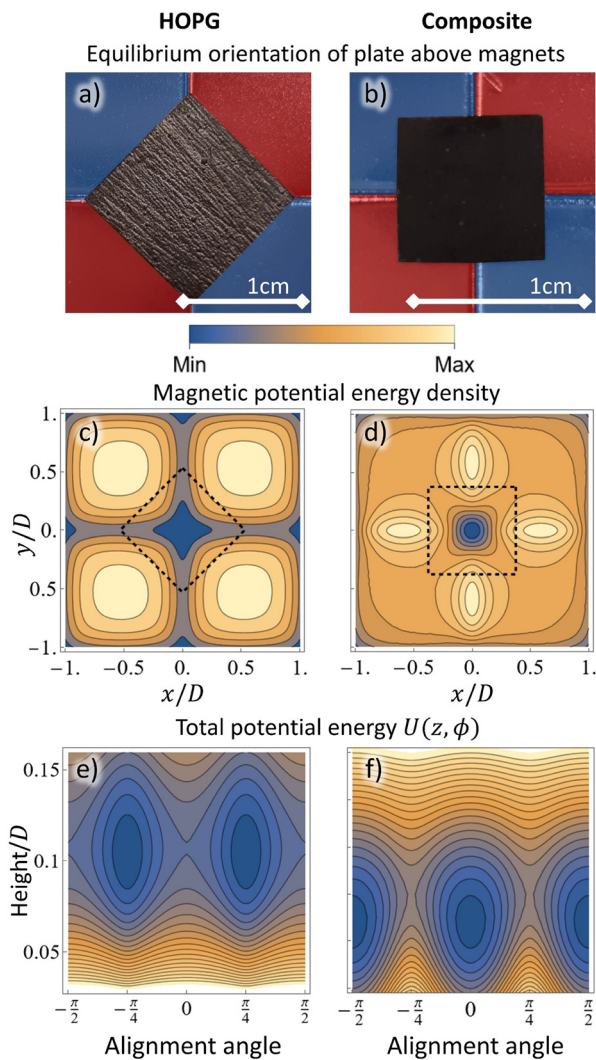

Total potential energy $U(z, \phi)$

FIG. 2. Re-orientation of diamagnetic slabs for HOPG (left) and composite graphite (right). (a) and (b) Photographs of levitated slabs above four cubic magnets with side lengths $D = 12.7$ mm. The checkerboard magnet array is shown in false color, with North red and South blue. In (a) the HOPG with dimensions $12.4 \times 12.4 \times 0.7$ mm^3 is oriented diagonally with respect to the magnets, whereas in (b) the composite graphite with dimensions $8.5 \times 8.6 \times 0.6$ mm^3 orients in line with the magnets. (c) and (d) Contours of the magnetic potential energy density Eq. (1) as a function of the lateral position of its center of mass. The dashed lines represent a slab with side lengths $0.75D$. In (c), anisotropic susceptibility of HOPG means that the z-component of the magnetic field contributes five times as much to the potential energy as the x, y-components. Thus, the HOPG orients diagonally, which minimizes overlap with the B_z-component. The composite graphite in (d) has an isotropic effective susceptibility which weights all components of the magnetic field evenly. To minimize overlap with the total magnetic field, the slab orients in line with the magnets. (e) and (f) Total potential energy as a function of orientation and height, for a slab of side length $0.75D$. In (e), for HOPG the density of 2070 kg/m^3 is used for calculating the gravitational potential. The energy minima occur when the slab is aligned at $\pi/4$ relative to the magnets, matching our observations. In (f), the energy of the composite graphite with the density of 1550 kg/m^3 is minimized when the slab is in line with the magnets. The composite levitates lower than HOPG, due to its lower effective susceptibility. Note that (c)–(f) are individually normalized, so the color scale cannot be directly compared between plots.

Here, χ_j are the components of the magnetic susceptibility tensor, B_j are the components of the magnetic field, and μ_0 is the vacuum permeability. The integral is over the volume $\mathcal{V}$ of the slab, which depends on its levitation height z and orientation ϕ. The susceptibility of pyrolytic graphite is highly anisotropic: $\chi_j^{\text{pyro}} = -(85, 85, 450) \times 10^{-6}$, and thus, the slab orients itself primarily to avoid the z-component of the magnetic field. The composite graphite, on the other hand, has uniform susceptibility and orients itself to avoid all magnetic field components equally.[16] We estimate this to be $\chi_j^{\text{comp}} = -(90, 90, 90) \times 10^{-6}$, based on the volume fraction of graphite. We plot the magnetic potential energy densities in Figs. 2(c) and 2(d), which we see accounts for the difference in orientation.

We can further study the difference between the two materials by evaluating the total potential energy, which is the sum of the magnetic and gravitational components. We graph this for pyrolytic and composite graphite in Figs. 2(e) and 2(f), which clearly show the difference in orientation. We can see that the composite graphite experiences a much looser angular confinement. The composite also levitates at smaller heights as compared to the HOPG. There are several effects which contribute to the different levitation height, namely, the lower effective susceptibility of the composite, its graphite mass fraction of 57%, and the density of the wax. These factors also influence the shape of the trap, as we discuss further in the supplementary material.

We note that these observations seem to disagree with those of Chen *et al.*,[16] which reported composite resonators to orient themselves similarly to pyrolytic graphite. A more detailed analysis in our supplementary material does not find a regime where such orientation is expected. One likely explanation is the geometry of the magnets. In our experiment shown in Figs. 2(a) and 2(b), the chamfering is small compared to the size of the magnets and graphite slabs; hence, we assumed the magnets to be perfect cubes in our analysis. However, in Chen *et al.* their magnets show significant chamfering, comparable to the size of their composite slabs. Given how shallow the composite potential is in Fig. 2(f), it is likely that this could be distorted by such changes to the magnet geometry. Another explanation could be that some unknown factor is causing slight orientation of the particles in their composite.

The composite's trapped dynamics were characterized using the setup shown in Fig. 1(c). The insulating resonator is levitated by an alternating polarity checkerboard magnet array made up of four NdFeB magnets. They are rigidly held within a holder that is mounted on a small optical breadboard. The breadboard itself sits on four vibration isolation supports. The velocity and displacement of the resonator are monitored by an interferometric displacement sensor (SmarAct PICOSCALE Interferometer). It is based on a compact Michelson interferometer and enables high-precision measurement of the position (and using numerical differentiation, also the velocity), in real time with a resolution of picometers at a high bandwidth. The sensor of the PICOSCALE is fixed to a five-axis ultra-high vacuum-compatible motorized stage. The whole structure is placed in a vacuum chamber, which is evacuated by a system consisting of a turbopump, an associated roughing pump, and an ion pump. During the measurement periods, the turbopump is switched off to avoid mechanical vibrations, while the ion pump operates continuously to maintain a high vacuum. To isolate the setup from vibrations, the vacuum chamber and ion pump are supported by a damped and vibration-isolated optical table, and the turbopump is supported by a separate vibration-

damped and isolated platform. The insulating resonator levitates above a checkerboard of four permanent magnets, with a small mirror placed on top of the slab in order to read out its position and velocity with a PICOSCALE interferometer. This setup is most sensitive to the slab's vertical oscillation, whose frequency is observed to be 18.95 Hz. This frequency matches simulations of the potential in Fig. 2(d). We actuate the system using a coil situated just above the graphite. A current flowing through this coil generates a magnetic field along its vertical axis, which perturbs the field generated by the magnets and, thus, exerts a force on the graphite. As discussed in the supplementary material, the force exerted by the coil depends only on the magnitude of the applied voltage, not its sign. When applying voltage signals to the coil, we, thus, operate around a DC shift, allowing us to apply both positive and negative forces. When performing measurement at high vacuum only the ion pump is left on, allowing us to maintain vacuum while minimizing vibrations. We refer to the supplementary material for further details on the setup.

To study the eddy damping in our composite resonator, we drive the vertical mode using the coil close to the resonance frequency of 18.95 Hz and then measure the ringdown at a pressure of 1.2×10^{-6} mbar for 10 000 s, as shown in Fig. 3. The velocity of a damped resonator decays exponentially as $v(t) \propto e^{-\pi f_0 t/Q}$, where f_0 is the natural frequency of the vertical mode. By fitting the envelope of measured velocity, we find the quality factor of vertical mode $Q \sim 1.58 \times 10^5$ for the 8 mm square composite plate.

Our measured damping rate is three orders of magnitude smaller than HOPG with engineered slots,[14,15] showing the effectiveness of composite materials in suppressing eddy currents. Moreover, the damping rate is almost one order of magnitude lower than that of the composite with the same particle size measured in Ref. 16 (see the supplementary material for a detailed comparison). This demonstrates that the insulating silica shell is indeed suppressing the flow of eddy currents between neighboring graphite particles, leading to almost an order of magnitude increase in quality factor.
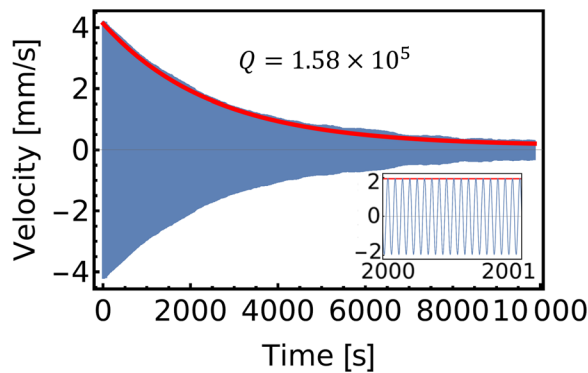

FIG. 3. Ringdown of the composite graphite resonator at a pressure of 1.2×10^{-6} mbar. The blue line shows velocity as measured by the interferometer. The inset zooms-in over a span of 1 s. The red curve denotes the fitted envelope, from which we find a damping rate of $\gamma \sim 7.4 \times 10^{-4}$ Hz, corresponding to a quality factor of $Q \sim 1.58 \times 10^5$. This is almost an order of magnitude smaller than the damping rate for other graphite composites with similar particle sizes (11 ± 2 μm).[16] This demonstrates that the insulating silica shell is effectively suppressing eddy currents between neighboring graphite particles.

Optomechanical applications of graphite composites will invariably require feedback cooling.[19] Aided by the electromagnetic coil above the levitated resonator, we apply feedback forces to cool the vertical motion. The feedback signal is generated from the real-time measured velocity by a Red Pitaya FPGA. To suppress noise and isolate the vertical mode, the velocity is bandpass filtered using a finite impulse response (FIR) filter. The filter and electronics have an intrinsic delay which we find to be approximately 7.6 periods of the 18.95 Hz oscillation signal. The FPGA, thus, also applies a variable time delay, allowing us to make sure velocity feedback is applied with the correct phase relative to the composite's motion. The signal from the FPGA is then amplified and applied to the coils. Further details on the feedback scheme are provided in the supplementary material.

For theoretical analysis, we approximate the vertical motion as a one-dimensional harmonic oscillator with a thermal drive. This approximation should be valid for small oscillations, where coupling to other motional modes should not be significant. Considering the velocity feedback, the equation of motion is

$$\ddot{x}(t) + \gamma \dot{x}(t) + \omega_0^2 x(t) + \Gamma_v \dot{x}(t-\tau) = \sqrt{\frac{2\gamma k_B T}{m}}\xi(t), \qquad (2)$$

where dots denote the time derivative. The vertical position of the oscillator is given by x. The oscillator has resonant frequency $\omega_0 = 2\pi f_0$, damping rate γ, and mass m. The temperature of the thermal bath is T, and k_B is Boltzmann's constant. The bath is modeled as Gaussian white noise $\xi(t)$, with autocorrelation $\langle \xi(t)\xi(t') \rangle = \delta(t-t')$. The feedback strength is given by Γ_v, which is applied with some time delay τ. This corresponds to a feedback force of $m\Gamma_v \dot{x}(t-\tau)$. In the supplementary material, we show that this has power spectral density

$$S_{xx}(\omega) = \frac{2k_B T \gamma/m}{\left[\omega_0^2 - \omega^2 + \omega\Gamma_v \sin(\omega\tau)\right]^2 + \left[\omega\gamma + \omega\Gamma_v \cos(\omega\tau)\right]^2}. \tag{3}$$

This formula is valid when $n - 1/4 \lesssim \tau f_0 \lesssim n + 1/4$, where f_0 is the oscillator frequency and n is an integer. In this regime, the time-delay is such that the applied feedback opposes the system's velocity. Otherwise the feedback acts to amplify the velocity, causing unbounded heating of the system.

To characterize the effectiveness of feedback in this system, we performed delayed velocity feedback cooling experiments at moderate ($\sim 1 \times 10^{-2}$ mbar) and low ($\sim 1 \times 10^{-6}$ mbar) pressures, with varying time delays and feedback strengths. The measured power spectral densities are shown in Fig. 4, which match closely with Eq. (3). We describe the feedback using feedback strength Γ_v(Hz) and dimensionless time delay $\tilde{\tau} = \tau f_0$, where f_0 is the natural frequency in the magnetic trap. At moderate pressures, we can estimate the value of γ by fitting to the PSD. At low pressures, the PSD is very narrow, so we estimate γ using ring-down measurements. The parameter Γ_v is fit from the experimental data. For the time delay τ, we first find an approximate value using our measured delay and the manual delay added by the FPGA and then fit τ within one period deviation of this. It is also necessary to fit the overall scale of the PSD. This scale fitting accounts for the fact that Eq. (2) models a point particle following ideal Brownian motion, whereas our system consists of a three-dimensional extended plate. Measurements at the moderate pressure took 20 min,
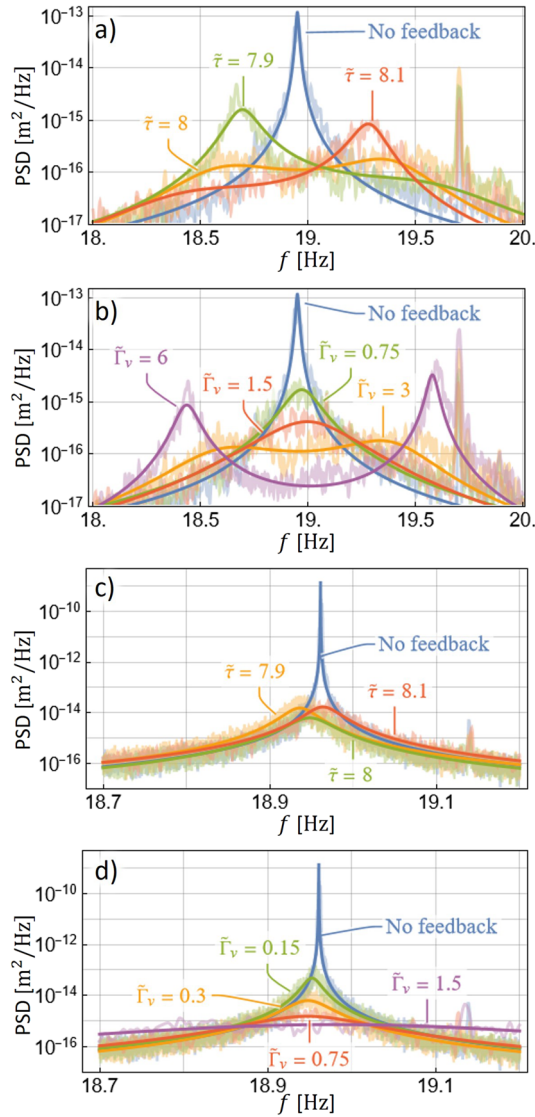
FIG. 4. Power spectral densities at (a) and (b) moderate pressure 10^{-2} mbar and (c) and (d) low pressure 10^{-6} mbar. We parameterize these with the feedback strength Γ_v (Hz) and dimensionless time delay $\tilde{\tau} = \tau f_0$, where f_0 is the natural frequency (Hz). The noisy traces are the experimental data, smoothed using Welch's method. The curves are fittings to Eq. (3), which show good agreement with theory. In (a) and (c), we fix $\Gamma_v = (3, 0.75)$ Hz, respectively, and vary the time delay. In (b) and (d), we fix $\tilde{\tau} = 8$ and vary the feedback strength. We note the presence at moderate pressure of other modes. Sidelobes appear due to the significant time delay in the system. At low pressure, the peak is significantly narrowed, and feedback cooling is able to decrease the temperature by three orders of magnitude. All fitting parameters are provided in the supplementary material.

while at low pressure, we required 7 h to resolve the peak. As we show in the supplementary material, at low pressure without feedback, the resonance frequency drifts slightly during this time which may be caused by the thermal expansion of the composite plate.

The temperature is defined as being proportional to the integrated area under the PSD. We find that cooling is strongest when τ is

an integer number of periods, which from Eq. (2) means that the feedback is directly opposing the velocity. When τ deviates from an integer value the PSD broadens and the peak shifts. At higher pressures with strong feedback strength, the time delay leads to visible sidelobes. Increasing the strength of the feedback leads to stronger cooling and larger sidelobes at higher pressure. At low pressure, with a time delay of 8 periods and a feedback strength of $\Gamma_v = 0.75$ Hz, we attain three orders of magnitude decrease in the temperature. We note that Brownian motion is typically studied for spherical objects. Brownian motion for non-spherical objects yields shape-dependent anisotropic diffusion,[20] which means that estimating the effective mass and absolute motional temperature through $\langle x^2 \rangle$ is difficult. We do the measurements following extended periods for the system to rest, which leads us to suppose that the system without feedback is in thermal equilibrium with the environment at 300 K and so the minimum temperature could be $T \sim 320$ mK. We refer to the supplementary material for further discussion of the experimental data and analysis.

In conclusion, we demonstrate a magnetically levitated centimeter-size composite resonator by mixing the silica-coated graphite particles with wax. The insulating coating on the graphite prevents eddy currents from flowing between adjacent particles, significantly reduces eddy damping, and provides a route to engineer larger motional Q-factors. We report the cooling of vertical motional mode at different delays and feedback strengths, with good agreement between experiment and theory. At suitable feedback conditions, we realize strong cooling of the centimeter-sized resonator by three orders of magnitude decrease in the center-of-mass temperature. In future work, larger Q-factors could be attained by further reducing the graphite particle sizes and using filtering to remove stray large particles. There are also schemes for cooling low frequency resonators further toward their ground state.[21,22] We note that one does not need to approach the ground state for the demonstrated resonator to be useful as a sensor. The acceleration sensitivity of a thermal noise limited resonator can be estimated as $\sqrt{S_a} = \sqrt{4k_B T \omega_0 / mQ}$.[11] For our massive high-Q resonator at $T = 320$ mK, the acceleration sensitivity can reach $\sim 1.7 \times 10^{-12} g/\sqrt{\text{Hz}}$, which is more precise than research grade atomic gravimeters,[23] the latter which achieve $\sim 2.2 \times 10^{-9} g/\sqrt{\text{Hz}}$, where g is the gravitational acceleration. This work is an initial step toward the preparation of quantum states of motion of large objects and shows the potential of our composite resonator for fundamental quantum physics and ultrahigh precision sensing.

See the supplementary material for details of the fabrication and characterization of the resonators, description of the setup, measurement and simulation of Q factors, theory of orientation of the resonators, theory and simulation of delayed feedback cooling, and measurement and fitting of the PSDs.

AUTHOR DECLARATIONS
Conflict of Interest

The authors have no conflicts to disclose.

Author Contributions

S. Tian: Conceptualization (equal); Data curation (equal); Formal analysis (equal); Investigation (equal); Methodology (equal); Software (equal); Writing – original draft (equal); Writing – review & editing (equal). **K. Jadeja:** Conceptualization (equal); Data curation (equal); Formal analysis (equal); Investigation (equal); Methodology (equal); Writing – original draft (equal); Writing – review & editing (equal). **D. Kim:** Formal analysis (equal); Investigation (equal); Methodology (equal); Software (equal); Writing – original draft (equal); Writing – review & editing (equal). **A. Hodges:** Formal analysis (equal); Investigation (equal); Methodology (equal); Software (equal); Writing – original draft (equal); Writing – review & editing (equal). **G. C. Hermosa:** Formal analysis (equal); Investigation (equal); Methodology (equal); Writing – original draft (equal); Writing – review & editing (equal). **C. Cusicanqui:** Formal analysis (equal); Investigation (equal); Software (equal); Writing – original draft (equal); Writing – review & editing (equal). **R. Lecamwasam:** Conceptualization (equal); Formal analysis (equal); Investigation (equal); Methodology (equal); Software (equal); Writing – original draft (equal); Writing – review & editing (equal). **J. E. Downes:** Conceptualization (equal); Investigation (equal); Methodology (equal); Writing – original draft (equal); Writing – review & editing (equal). **J. Twamley:** Conceptualization (equal); Formal analysis (equal); Investigation (equal); Methodology (equal); Project administration (equal); Software (equal); Supervision (equal); Writing – original draft (equal); Writing – review & editing (equal).

DATA AVAILABILITY

The data that support the findings of this study are available from the corresponding author upon reasonable request.

REFERENCES

[1]L. Magrini, P. Rosenzweig, C. Bach, A. Deutschmann-Olek, S. G. Hofer, S. Hong, N. Kiesel, A. Kugi, and M. Aspelmeyer, "Real-time optimal quantum control of mechanical motion at room temperature," Nature **595**, 373–377 (2021).

[2]C. Gonzalez-Ballestero, M. Aspelmeyer, L. Novotny, R. Quidant, and O. Romero-Isart, "Levitodynamics: Levitation and control of microscopic objects in vacuum," Science **374**, eabg3027 (2021).

[3]G. Winstone, M. Bhattacharya, A. A. Geraci, T. Li, P. J. Pauzauskie, and N. Vamivakas, "Levitated optomechanics: A tutorial and perspective," arXiv:2307.11858 (2023).

[4]D. C. Moore and A. A. Geraci, "Searching for new physics using optically levitated sensors," Quantum Sci. Technol. **6**, 014008 (2021).

[5]J. Young, H. Biggs, S. Yee, and H. ElBidweihy, "Optical control and manipulation of diamagnetically levitated pyrolytic graphite," AIP Adv. **9**, 125038 (2019).

[6]M. Fujimoto and M. Koshino, "Diamagnetic levitation and thermal gradient driven motion of graphite," Phys. Rev. B **100**, 045405 (2019).

[7]S. Yee, L. Oney, T. Cosby, D. P. Durkin, and H. ElBidweihy, "Photothermal actuation of levitated pyrolytic graphite revised," APL Mater. **9**, 101107 (2021).

[8]M. Ewall-Wice, S. Yee, K. DeLawder, S. R. Montgomery, P. J. Joyce, C. Brownell, and H. ElBidweihy, "Optomechanical actuation of diamagnetically levitated pyrolytic graphite," IEEE Trans. Magn. **55**, 1–6 (2019).

[9]X. Chen, A. Keşkekler, F. Alijani, and P. G. Steeneken, "Rigid body dynamics of diamagnetically levitating graphite resonators," Appl. Phys. Lett. **116**, 243505 (2020).

[10]M. D. Simon and A. K. Geim, "Diamagnetic levitation: Flying frogs and floating magnets (invited)," J. Appl. Phys. **87**, 6200–6204 (2000).

[11]C. Timberlake, G. Gasbarri, A. Vinante, A. Setter, and H. Ulbricht, "Acceleration sensing with magnetically levitated oscillators above a superconductor," Appl. Phys. Lett. **115**, 224101 (2019).

[12]M. Rademacher, J. Millen, and Y. L. Li, "Quantum sensing with nanoparticles for gravimetry: When bigger is better," Adv. Opt. Technol. **9**, 227–239 (2020).

[13]P. Yin, R. Li, C. Yin, X. Xu, X. Bian, H. Xie, C.-K. Duan, P. Huang, J.-H. He, and J. Du, "Experiments with levitated force sensor challenge theories of dark energy," Nat. Phys. **18**, 1181–1185 (2022).

[14]P. Romagnoli, R. Lecamwasam, S. Tian, J. E. Downes, and J. Twamley, "Controlling the motional quality factor of a diamagnetically levitated graphite plate," Appl. Phys. Lett. **122**, 94102 (2023).

[15]H. Xie, Y. Li, R. Li, Y. Leng, Y. Chen, L. Wang, D. Long, X. Bian, C.-K. Duan, P. Yin, P. Huang, and J. Du, "Suppressing mechanical dissipation of diamagnetically levitated oscillator via engineering conductive geometry," Phys. Rev. Res. **5**, 013030 (2023).

[16]X. Chen, S. K. Ammu, K. Masania, P. G. Steeneken, and F. Alijani, "Diamagnetic Composites for High-Q Levitating Resonators," Adv. Sci. **9**, 2203619 (2022).

[17]B. Semenenko and P. Esquinazi, "Diamagnetism of bulk graphite revised," Magnetochemistry **4**, 52 (2018).

[18]Y. Kim, Y. Qian, M. Kim, J. Ju, S.-H. Baeck, and S. E. Shim, "A one-step process employing various amphiphiles for an electrically insulating silica coating on graphite," RSC Adv. **7**, 24242–24254 (2017).

[19]M. Debiossac, D. Grass, J. J. Alonso, E. Lutz, and N. Kiesel, "Thermodynamics of continuous non-markovian feedback control," Nat. Commun. **11**, 1360 (2020).

[20]Y. Han, A. M. Alsayed, M. Nobili, J. Zhang, T. C. Lubensky, and A. G. Yodh, "Brownian motion of an ellipsoid," Science **314**, 626–630 (2006).

[21]L. S. Walker, G. R. Robb, and A. J. Daley, "Measurement and feedback for cooling heavy levitated particles in low-frequency traps," Phys. Rev. A **100**, 63819 (2019).

[22]K. Streltsov, J. S. Pedernales, and M. B. Plenio, "Ground-state cooling of levitated magnets in low-frequency traps," Phys. Rev. Lett. **126**, 193602 (2021).

[23]T. Zhang, L.-L. Chen, Y.-B. Shu, W.-J. Xu, Y. Cheng, Q. Luo, Z.-K. Hu, and M.-K. Zhou, "Ultrahigh-sensitivity Bragg atom gravimeter and its application in testing Lorentz violation," Phys. Rev. Appl. **20**, 014067 (2023).